Turkish Journal of Electrical Engineering & Computer Sciences

http://journals.tubitak.gov.tr/elektrik/

Research Article

Turk J Elec Eng & Comp Sci
(2019) 27: 4340 – 4353

doi:10.3906/elk-1901-216

A new technique for the measurement and assessment of carotid artery wall vibrations using ultrasound RF echoes

Samrand SHARIFI[1], **Hamid BEHNAM**[2,*], **Zahra ALIZADEH SANI**[3]

[1]Department of Biomedical Engineering, Science and Research Branch, Islamic Azad University, Tehran, Iran

[2]Department of Biomedical Engineering, School of Electrical Engineering, Iran University of Science and Technology, Tehran, Iran

[3]Rajaie Cardiovascular Medical and Research Center, Iran University of Medical Sciences, Tehran, Iran

Received: 29.01.2019 • **Accepted/Published Online:** 27.04.2019 • **Final Version:** 26.11.2019

Abstract: Atherosclerosis is known as the leading cause of heart attacks and brain strokes. One of the symptoms of this disease is the reduction of artery wall motion caused by age. This study presents a novel method to extract high frequency components of wall motion, wall vibrations, based on discrete wavelet transform. The fractal dimension, largest Lyapunov exponent, and spectral entropy are then analyzed to indicate the chaotic behavior in wall vibrations. Phase information from demodulated radiofrequency signals is extracted and the entropy of phase-difference is computed as a statistical measure for better characterization of the artery wall tissue. The results show that these features correlate with age ($P < 0.001$) and also increase with age. The phase-difference entropy also shows significant correlation with age ($r = 0.34$, $P < 0.001$). The measurement results indicate that while age increases, vibrations of the artery wall are irregular and represent chaotic behavior. Our results raise hopes that the proposed approach may be effective in diagnosing atherosclerosis.

Key words: Carotid wall, fractal dimension, Lyapunov exponent, entropy, phase information, radiofrequency signals

1. Introduction

Physical stiffening of the carotid artery is the most important stroke and death risk factor in industrialized countries [1]. The stiffness of plaques can be estimated by stiffness meter to clarify the correlation between plaque stiffness and preoperative carotid ultrasonographic findings, and to predict the stiffness of plaques before surgery [2]. Diagnosis of this disease in the early stages can be very helpful [3]. Previous studies using radiofrequency (RF) signal analysis have indicated that there is a relationship between changes of the carotid artery wall and coronary artery diseases [4]. Arterial stiffness may be accompanied by changes in the elasticity of the artery wall. There are different imaging methods for diagnosing atherosclerosis like computed tomography (CT), magnetic resonance imaging (MRI), and ultrasonic imaging [5–7]. Larsson et al. [8] used ultrasound speckle tracking for carotid strain assessment in arterial stiffness and cardiovascular diseases. They evaluated the contrast carotid strain assessment by speckle tracking applied on clinical and high-frequency ultrasound images in vitro. A significantly larger bias and root mean square error were found for circumferential strain estimation for clinical ultrasound images compared to high frequency ultrasound images, but no significant difference was found for radial and longitudinal strain. Optical flow methods have also been used to quantify

*Correspondence: behnam@iust.ac.ir

plaque motion and shear strain during the cardiac cycle [9]. A noninvasive method that examines the mechanical properties of soft tissue, called acoustic radiation force impulse (ARFI) imaging, has been developed as a new modality for atherosclerotic plaque characterization using phantoms and atherosclerotic pigs, but the technique has yet to be validated in vivo in humans [10]. Huang et al. [11] studied the textural information of strain rate images in ultrasound carotid elastography and evaluated the feasibility of using the textural features in discriminating stable and vulnerable plaques with magnetic resonance imaging. They indicated that the use of texture analysis in plaque classification is feasible and that larger local deformations and higher levels of complexity in deformation patterns are more likely to occur in vulnerable plaques.

Although the accuracy of these methods in detecting parameters like artery diameter is high, there are many problems in using these methods, such as physical and neural problems of the patient while imaging. Also, artery stiffness does not change the diameter of the lumen in initial stages. Therefore, we should look for methods to diagnose this disease in its initial stages. In different articles, various noninvasive methods have been investigated to estimate the elasticity of the artery wall or determine wall thickness during one heart beat by tracking different points on the wall. Some of these methods, including pulse wave velocity (PWV), have low resolution because of the considerable distance of the measurement point from the heart [12].

The changes in blood pressure and flow move the artery wall in a radial orientation during a cardiac cycle. Atherosclerosis may affect the motion of the artery wall and reduce the ability of the artery to expand and contract in response to blood pressure changes [13–15]. The radial motion of the carotid wall using image-based methods, which are applied to B-mode ultrasound image sequences, is estimated quantitatively. Different procedures have employed a phased tracking method for ultrasound RF signals to track the wall motion in real time [16]. The phased tracking method was first proposed to evaluate elasticity of the artery wall [17]. In this method, minimal changes in wall shape can be detected based on the velocity estimation accuracy. The wall motion velocity in radial orientation is estimated based on the phase shift of echoes, which is related to changes in the delay of ultrasound beams between the ultrasound probe and the artery wall. In the methods proposed by Kanai et al. [18], Hasegawa et al. [19], and Koiwa et al.[20], a set of two points is determined along an ultrasound beam and the change in the thickness of the layer between these two points is estimated.

Among the mentioned methods, it can be seen that none of them are able to extract wall vibrations; moreover, they can only be applied when atherosclerosis has occurred. Also, most of the above methods are based on B-mode ultrasound images obtained by demodulating RF echo signals, which in turn are calculated using the RF signals envelope. Therefore, there are several machine-dependent processing steps that should be applied to the RF signals to calculate corresponding B-mode images. These processing steps may cause information loss from the signal. In recent years, many studies have been conducted in the field of ultrasound tissue characterization using unprocessed RF signals, which are rich in information [21–27]. However, the major problem in processing RF data is the interaction between tissue and acoustic waves, which might be difficult to understand. Most studies are performed based on statistical characteristics of RF signals' amplitude and envelope images. In addition, limited analysis is performed on the statistical properties of the ultrasound images' phase and this could be due to the stochastic nature of the phase information. Vascular aging, as an independent risk factor for cardiovascular diseases like atherosclerosis, is also accelerated by other coexisting cardiovascular risk factors such as hypertension and diabetes [28].

In this work, in order to study changes in the internal wall radial motion of the carotid artery of the people in a dataset, a novel approach based on entropy of phase-difference from RF signals is presented. In addition, the vibrations of the posterior carotid artery wall based on radial motion are extracted using discrete

wavelet transform. Due to the nonlinear dynamical nature of biologic systems and the fact that cardiovascular systems are more complicated than a linear system and represent nonstatic behavior, nonlinear features can represent chaotic dynamic characteristics of artery wall vibrations, which can be the result of aging. Hence, we used features such as fractal dimension, spectral entropy, and largest Lyapunov exponent to compare the nonlinear dynamics of vibrations with the subjects' age changes.

2. Materials and methods

The block diagram of the proposed technique is shown in Figure 1. In this study, we attempted to extract carotid wall vibration signals with small amplitudes. These vibrations are superposed on the motion with large amplitudes. To extract the carotid wall vibrations, we used the wall motion tracking method. Then vibrations were obtained by removing the wall motion using the discrete wavelet transform method.

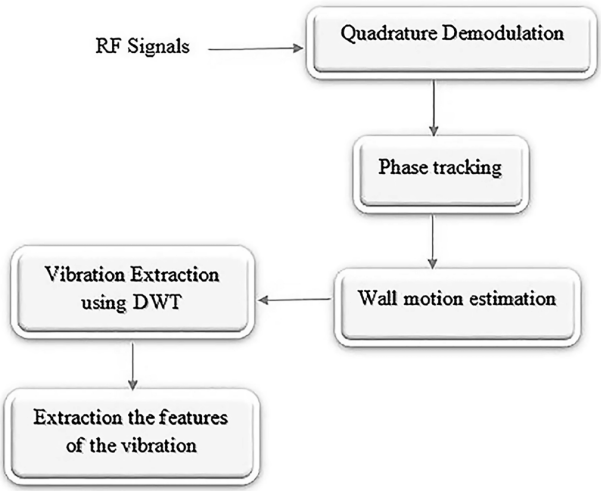

Figure 1. Block diagram of the proposed method.

2.1. Experimental data

In this study we used RF data of the right carotid arteries of 31 healthy volunteers. We asked participants to rest for 10 min so that their heart beat and blood pressure became stable. The position of the subjects and probe settings were such that it was assured that wall motion was due to blood flow. Efforts were made to minimize the motions of the patient, and subjects were asked to hold their breath and avoid swallowing.

In this work, a MyLab 60 (ESAOTE, Italy) ultrasound system equipped with an LA532 linear array probe (3–13 MHz) with frame rate of 60 frame/s was used. Each data record includes 355 frames containing 6–8 cardiac cycles. Thus, the right carotid artery is scanned longitudinally and the obtained RF signals are converted into matrix form using MATLAB. Dimensions of the matrices are $2526 \times 129 \times 355$. The number of sample points in the depth is 2526 and the number of RF echo lines is 129; 355 frames in 6 s are recorded for each individual.

2.2. Extracting motion of carotid artery wall

A phase tracking method based on RF signals is used, which is based on the phase change of the Hilbert transform of the received RF echo from two corresponding layers in subsequent frames. As can be seen in

Figure 2, RF pulses at a central frequency of f_0 and time interval of T are generated by the ultrasound probe and transmitted to the tissue, and then the returned echo is recorded by the same probe. The propagation delay, $\tau_1(n)$, between the probe and a reflector at the nth transmission (frame) depends on sound wave velocity, c_0, and the distance, $d_1(n)$, between the probe and the reflector according to Eq. (1) [29]:

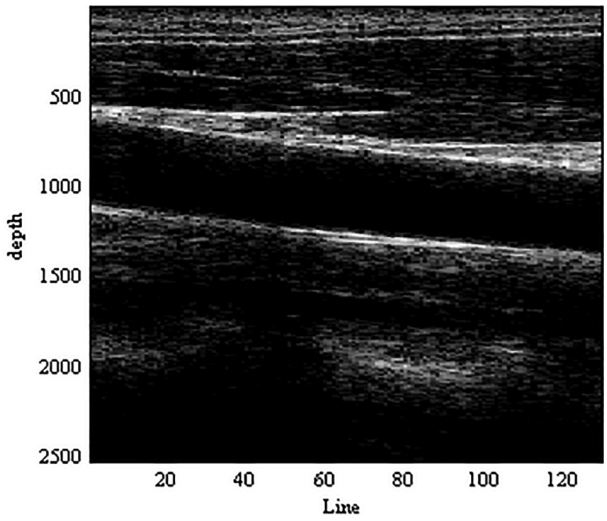

Figure 2. Estimation of radial displacement in the arterial wall.

$$\tau_1(n) = \frac{2d_1(n)}{c_0}(n = 1, 2, , N; N : numberoframes). \tag{1}$$

Phase $\theta_1(n)$ of the received echo is described by $\theta_1(n) = 2\pi\tau_1(n)f_0$ at central frequency f_0. Therefore, distances $d_1(n)$ and $d_1(n+1)$ between the ultrasound probe and the reflector in the nth and $(n+1)$th frames is given in Eqs. (2) and (3), respectively:

$$d_1(n) = \frac{c_0\tau_1(n)}{2} = \frac{c_0}{4\pi f_0}\theta_1(n), \tag{2}$$

$$d_1(n+1) = \frac{c_0\tau_1(n+1)}{2} = \frac{c_0}{4\pi f_0}\theta_1(n+1). \tag{3}$$

The average velocity of the reflector during a frame interval, T, is given in Eq. (4):

$$v_1 = \frac{d_1(n+1) - d_1(n)}{T} = \frac{c_0(\tau_1(n+1) - \tau_1(n))}{2T} = \frac{c_0}{4\pi f_0 T}\Delta\theta_1(n). \tag{4}$$

In order to obtain $\theta_1(n)$ of an RF echo, the Hilbert transform is applied to sampled RF echoes, which are windowed, and complex sampled signal z(n;x) along the ultrasound beam is obtained. Initial depth $x_1(1) \approx d_1(1)$ is manually defined for the position of the reflector at the first frame. When $x_1(1)$ is inside the interval of the echo returned from $d_1(1)$, the phase, $\angle z(n, x_1(n))$, which belongs to complex signal $z(n, x_1(n))$ in depth $x_1(n)$, corresponds to $\theta_1(n)$:

$$\theta_1(n) = \angle(n, x_1(n)). \tag{5}$$

We can calculate the time lag, $\hat{\delta}$, that maximizes cross-correlation between signals in the nth and $(n+1)$th frames. Then one of these signals is transferred with this amount of lag and the phase shift, $\Delta\theta_1(n)$, for two corresponding windows with period ΔT can be determined as follows:

$$\Delta\theta_1(n) = \theta_{HIL}(n+1) - \theta_{HIL}(n), \tag{6}$$

where $\theta_{HIL}(n+1)$ and $\theta_{HIL}(n)$ are the phases of the Hilbert transform of two corresponding layers in two subsequent frames, which are unwrapped to reduce the difference caused by phase jumps from π to $-\pi$. The average velocity is defined as in Eq. (7):

$$\hat{v}(x, t + \frac{\Delta T}{2}) = c_0 \frac{\Delta\theta_1(n)}{2w_0\Delta T}. \tag{7}$$

By multiplying the obtained velocity in time period ΔT, the next position of $\hat{x}(t)$ is estimated as in Eq. (8):

$$\hat{x}(t) = \hat{x}(t - \Delta T) + \hat{v}(x, t + \frac{\Delta T}{2}).\Delta T. \tag{8}$$

2.3. Discrete wavelet transform (DWT)

Wavelet transform provides the ability to decompose a signal into its frequency components while the location of these components on the time axis is also specified. This transform can be represented as follows [30]:

$$W_\phi X(a, b) =< x(t), \phi_{a,b}(t) >, \tag{9}$$

where $< ., . >$ denotes the inner product and $\phi_(a, b)(t)$ is the transferred and scale-adjusted version of the parent wavelet function, $\phi(t)$:

$$\phi_{a,b}(t) = |a|^{-\frac{1}{2}} \phi(\frac{t-b}{a}), \tag{10}$$

where a and b are translation and scale parameters, respectively. The wavelet transform is the result of correlation between the frequency content of the signal and wavelet function in different scales. In order to calculate the wavelet transform, the intent window is expanded/contracted and shifted and its product with the signal is integrated over time at each location. If parameters a and b become discrete, as shown in Eq. (11):

$$a = a_0^j, b = kb_0a_0^j, \tag{11}$$

where k and j are real numbers, then the wavelet function becomes discrete, as follows:

$$\phi_{j,k}(t) = a_0^{-\frac{j}{2}} \phi(a^{-j}t - kb_0), \tag{12}$$

where $\phi_{j,k}(t)$ is the base of the discrete wavelet transform. In discrete cases, filters with different cut-off frequencies are used to analyze the signal in different scales. As the signal passes high-pass and low-pass filters, its different frequencies are analyzed. In discrete cases, signal resolution is controlled by operations of the filters and the scale is changed through upsampling or downsampling. Selecting the wavelet transform and the number of decomposition levels using discrete wavelet transform is very important.

2.4. Largest Lyapunov exponent (LLE)

The Lyapunov exponent is a measure of how nearby trajectories converge or diverge. A positive number indicates that the behavior of a system is chaotic [31]. We assume that two points, x_0 and $x_0 + \Delta x_0$, in space are a function of time and each one generates a trajectory in space using a number of systemic equations. Then the separation of the two trajectories, Δx, would be a function of time as well. This separation is also a function of the initial position, whose shape is $\Delta x(x_0, t)$. For a chaotic dataset, function $\Delta x(x_0, t)$ operates irregularly. The average exponential tone of divergence of two trajectories that are adjacent at the beginning is determined using the following equation:

$$\lambda = \lim_{t\to\infty} \frac{1}{t} \frac{|\Delta x(x_0, t)|}{|\Delta x_0|}. \tag{13}$$

2.5. Spectral entropy (SpEn)

Spectral entropy describes the complexity of a time series spectrum quantitatively. Employing Shannon channel entropy gives an estimation of spectral entropy, where entropy is defined as follows:

$$E = -\sum_f P_f log(\frac{1}{P_f}), \tag{14}$$

where P_f is the probability density function at frequency f. Entropy is a measure of uncertainty at frequency f. Therefore, entropy can be used as a measure of system complexity [31].

2.6. Fractal dimension (FD)

The fractal dimension quantifies the degree of complexity of a system. It can also show irregular changes in a system. Fractal dimension is usually calculated using the Katz algorithm, which is the most effective method due to its simplicity and robustness. This feature is calculated as follows:

$$FD = \frac{log(N-1)}{log(N-1) + log(d/L)}, \tag{15}$$

where N is the total number of points in the processing interval, L is the length of the intent section (Euclidean distance between subsequent points of data), and d is the diameter of the intent section (Euclidean distance between first point and the furthest point in the intent section) [31]. The FD of each signal varies between 1 and 2, where 1 shows complete regularity or minimum energy and 2 indicates maximum irregularity or energy in the dynamic fluctuation components of the signal.

2.7. Statistical characteristics of RF echo phase

In this section, in order to study the statistical information of the RF signal phase, specific depth including lumen–intima and media–adventitia boundaries on the posterior carotid artery wall on a line is determined manually for each dataset of subsequent frames. Then the phase-difference of RF signals of the wall between subsequent frames is calculated. To this end, one line in all frames (line 80) and 100 samples along the depth are selected while the distance between each two samples along the depth is 0.3876 mm.

Our experimental data include ultrasound images of an ROI region of the carotid artery wall where each set of images including 355 frames is obtained from the same region of subsequent scans. In other words, the dimension of the matrix is 100×355. First, we extract the phase by applying Hilbert transform, and then phase-difference distribution is obtained by calculating entropy in a local neighborhood. In order to obtain the phase-difference, first the new matrix including the phase of RF signals is obtained, and then the phase-difference of signals in subsequent frames is calculated and the entropy of the phase-difference is obtained. Entropy can be used as a measure of system complexity, which is calculated as follows:

$$E(\Delta\phi) = -\sum_{i=1}^{N} p((\Delta\phi)_i) logp((\Delta\phi)_i). \tag{16}$$

In this equation, $E(\Delta\phi)$ is entropy, $\Delta\phi = [(\Delta\phi_1), , (\Delta\phi_N)]$ is the difference of phases, $N = n^2$ is the number of phase-differences in an n $\times$ n local neighborhood (e.g., in the case of a 9-by-9 neighborhood $N = 81$), and $p(\Delta\phi_i)$ is the probability density function (PDF) of phase-differences. The PDF function is estimated empirically from the histogram of phase-differences in an n $\times$ n local neighborhood.

3. Results and discussion

The right carotid artery RF data of 31 healthy volunteers including 19 men and 12 women (with age distribution of 37.54 ± 14.89 years) without a history of cardiovascular diseases, blood pressure, or diabetes were recorded. A sample of a recorded carotid artery wall is shown in Figure 3.

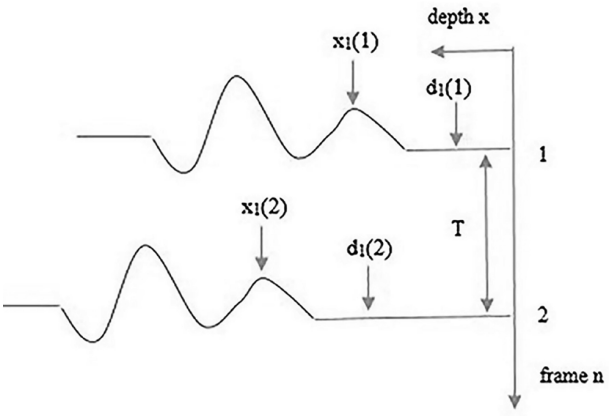

Figure 3. Sample of recorded carotid artery wall.

Given $\hat{x}(t)$, and the velocity, $\hat{v}(x, t + \frac{\Delta T}{2})$, according to Eqs. (7) and (8), the object's position as well as the motion velocity on large amplitude motion were determined simultaneously. The estimated wall motion for a subject is shown in Figure 4.

3.1. Extracting the vibration of the carotid wall using DWT

We aim to use DWT to extract the vibrations in the range of about a few millimeters that are superimposed on arterial wall motion. In this study, Daubechies wavelets transform (db10) is used as the mother wavelet. The Daubechies wavelets are a family of orthogonal wavelets defining a discrete wavelet transform and characterized

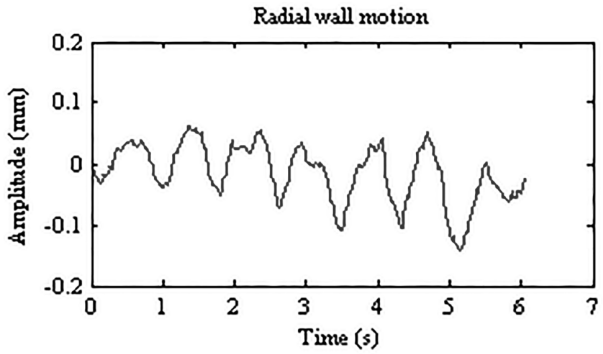

Figure 4. Extracted wall motion of a subject along with phase-tracking method.

by a maximal number of vanishing moments for some given support. With each wavelet type of this class, there is a scaling function (called the father wavelet), which generates an orthogonal multiresolution analysis. The db10 refers to the number of vanishing moments. The wall motion signal is decomposed in 6 steps; approximate and partial coefficients are obtained. By obtaining wavelet transform coefficients, the signal is reconstructed in approximate and partial subspaces V_j and W_j. The signal reconstructed in partial subspace W_5 contains high frequency components, i.e. wall vibrations, as shown in Figure 5.

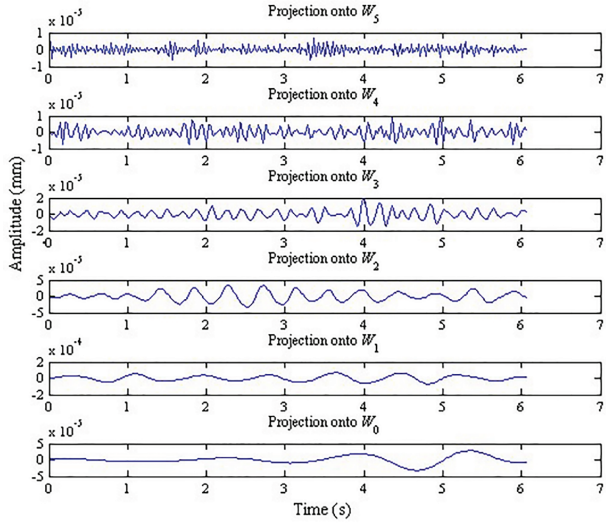

Figure 5. The reconstructed signals in partial subspace W_j .

3.2. Statistical analysis

The association of carotid wall vibration features with age were assessed by Pearson's correlation analysis. Pearson's correlation coefficient (r) is the covariance of two variables divided by the product of their standard deviations. We have used SPSS 22 for statistical analysis. Statistical significance is inferred at $P < 0.05$.

3.3. The effect of age on phase difference entropy of RF echo

Entropy images are reconstructed from RF signals of the carotid artery wall through time (frames). According to Eq. (4), it can be inferred that the phase-difference of RF signals is directly proportional to wall motion velocity. Therefore, by analyzing phase-differences for RF signals of the wall, changes in motion of the artery wall can be investigated. Finally, entropy is used to illustrate the complexity and irregularity of artery wall motion. Figure 6 shows entropy images for a young, a middle-aged, and an elderly participant.

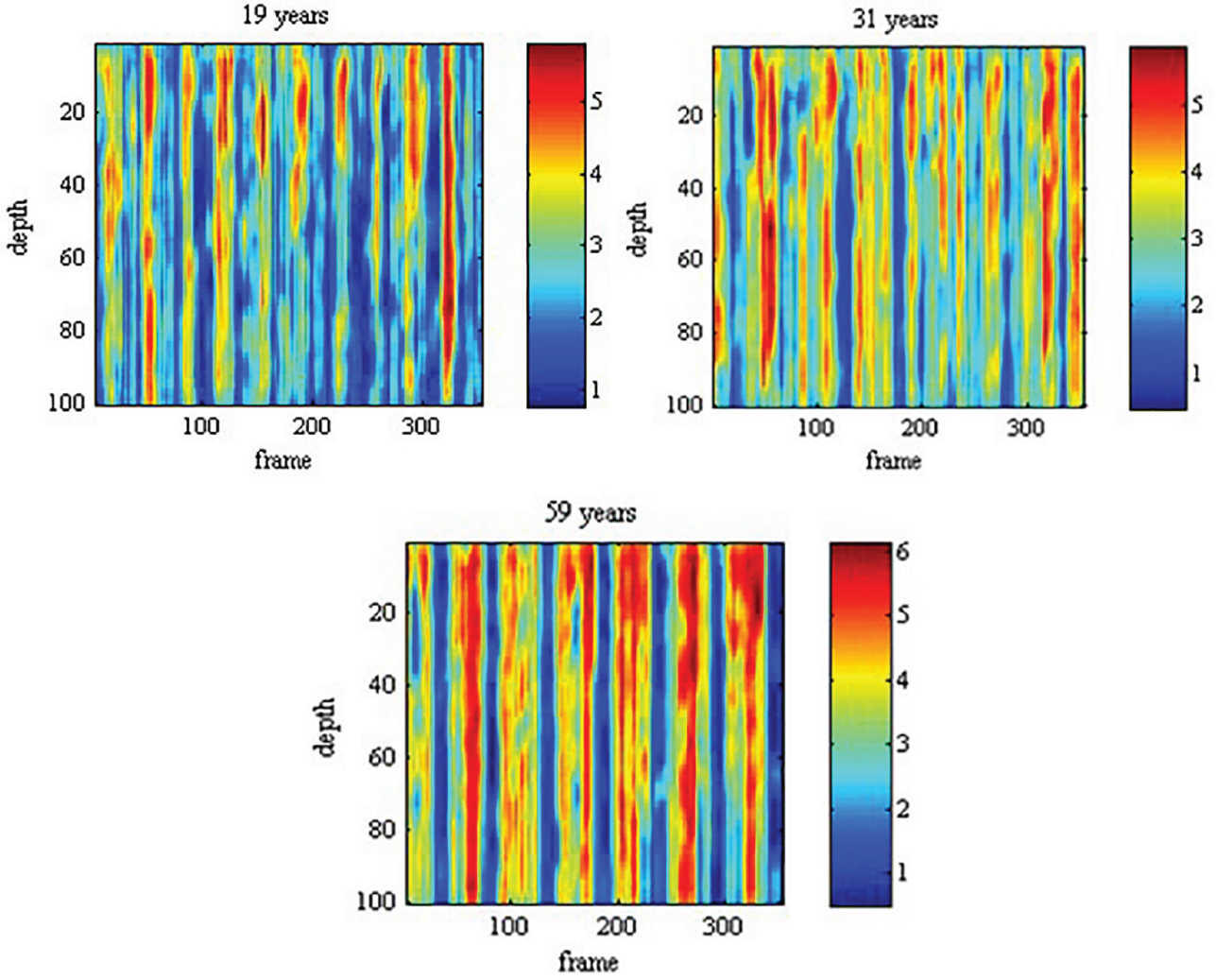

Figure 6. Entropy images for (a) a young, (b) a middle-aged, and (c) an elderly subject.

The obtained results for the calculated phase-differences show that the value of entropy for elderly subjects is sufficiently greater than those of younger ones. Applying our method, we noticed that the phase-difference is randomly distributed and the entropy is high while age increases. The relationship between average values of entropy image and age using Pearson correlation is shown in the Table ($r = 0.34$, $P = 5.38 \times 10^{-4}$). In addition, linear regression analysis using the age parameter related to average values of the entropy image is obtained. The average values of entropy are obtained as an independent parameter, which are affected by age.

To evaluate the carotid wall's changes with age, the subjects were investigated in two age groups (young and elderly subjects, considering the age of 50 as a threshold), including 6 elderly and 25 young people. Average values of entropy of phase-differences in 31 volunteers are shown as a box plot diagram in Figure 7a. Comparing the results as shown in Figure 7a verifies that the average entropy of phase-difference in the younger group is less than that in the elderly.

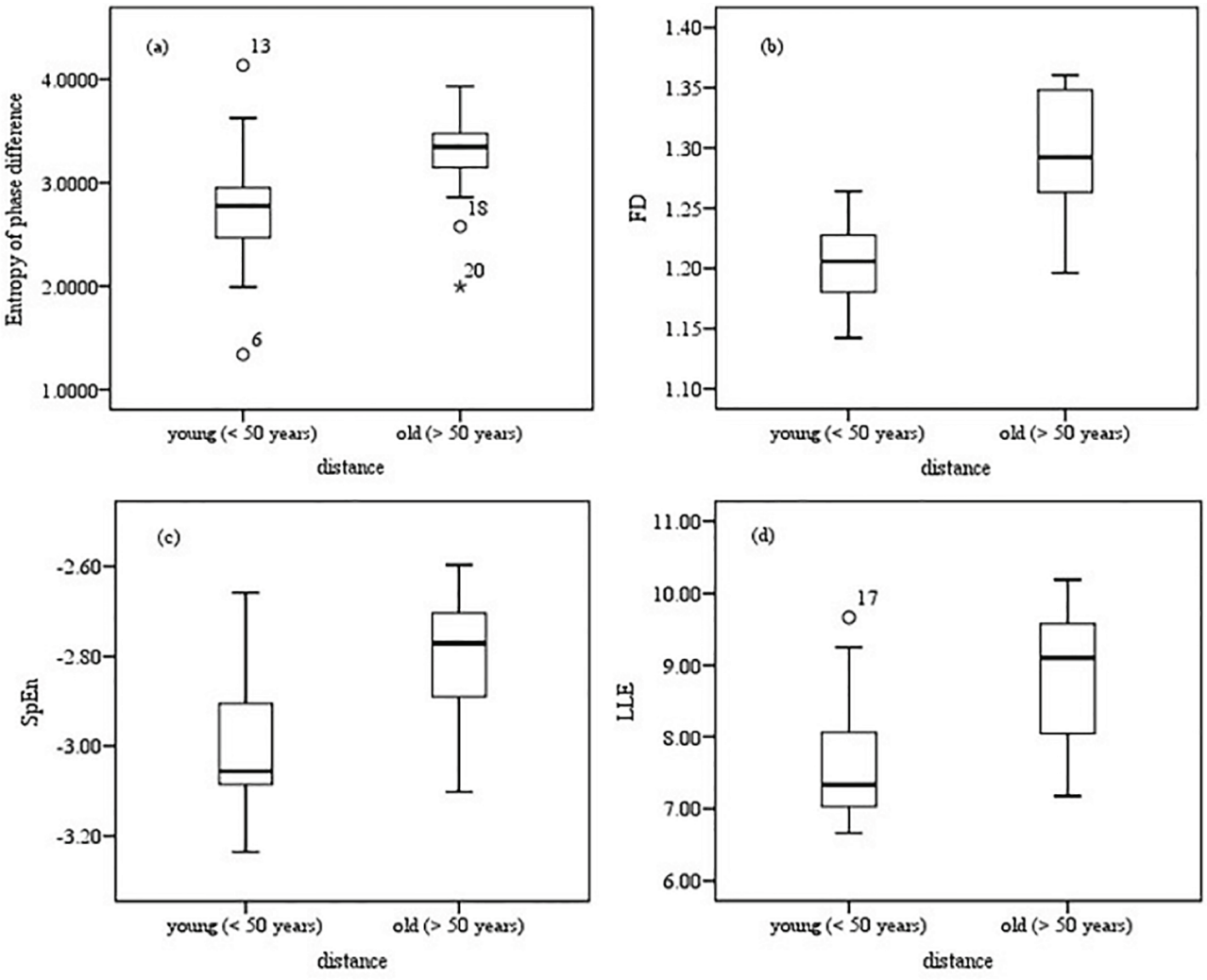

Figure 7. Result of the comparative measures between the two populations (young and elderly subjects, considering the age of 50 as a threshold) for (a) entropy of phase-difference (b) FD, (c) SpEn, and (d) LLE features, respectively.

3.4. The effect of age on nonlinear features of vibration signal

The vibrations of the artery wall are irregular while age increases, which can show chaotic behavior. In this section, the relationship between nonlinear features of vibrations and age is investigated to study the nonlinear dynamics of vibrations in the young and old groups. The values of nonlinear features including FD, LLE, and SpEn are shown as box plot diagrams in Figure 7b, Figure 7c, and Figure 7d.

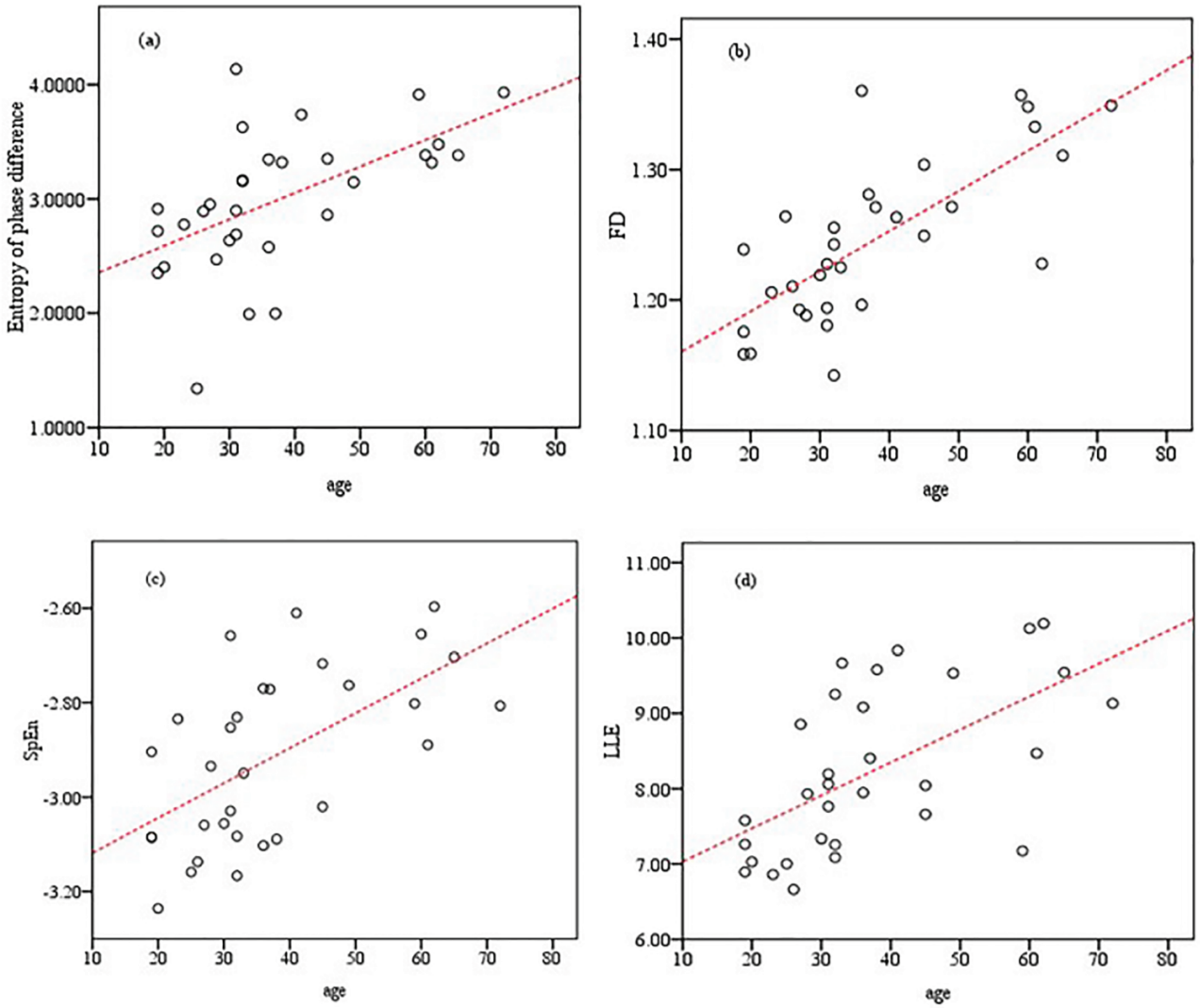

Figure 8. Correlation diagram of the values of (a) entropy of phase-difference, (b) FD, (c) SpEn, and (d) LLE features and age, respectively.

Comparing the results as shown in Figure 7b, Figure 7c, and Figure 7d indicates that these values are lower in the young group compared to the elderly group; this shows that while age increases, artery wall motion and high frequency vibrations of the wall are irregular and represent chaotic behavior. The average entropy of phase-difference is correlated with age and its value is higher in elderly subjects (> 50 years). In other words, the average entropy of phase-difference is highly correlated with age ($P < 0.001$). This is shown in Figure 8a.

Average values of nonlinear features (FD: $r = 0.73$, $P = 2 \times 10^{-6}$, SpEn: $r = 0.56$, $P = 9.76 \times 10^{-4}$, and LLE: $r = 0.60$, $P = 2.92 \times 10^{-4}$) are correlated with age as shown in the Table. These values are higher in elderly subjects (> 50 years). In other words, nonlinear features are highly correlated with age ($P < 0.001$). This is shown in Figure 8b, Figure 8c, and Figure 8d.

Some measures such as artery diameter, wall thickness, or artery stiffness are used to evaluate elasticity in heart cycles. Most of these measures require blood pressure and artery diameter in different phases of the

Table 1. Association between the average values of the image entropy and chaotic features of the wall vibration and subject age.

Features	r-value	P-value	$P < 0.05$
Average of the entropy image	0.34	5.38×10^{-4}	< 0.001
FD	0.73	2×10^{-6}	< 0.00001
SpEn	0.56	9.76×10^{-4}	< 0.001
LLE	0.60	2.92×10^{-4}	< 0.001

heart cycle. One of the most important reasons for error in determining carotid stiffness is measuring blood pressure in the brachial artery instead of the carotid artery. There are solutions such as synchronizing the blood pressure waveform and wall displacement, but a more accurate method is required to evaluate carotid wall stiffness.

In this study, we aimed to investigate a high frequency vibration signal that had been less studied in the literature. To this end, to consider nonlinear behavior of the cardiovascular system, nonlinear features like FD, LLE, and SpEn were extracted from vibration signals according to the age of the participants. The results showed that while age increases, the values of these features increased and they were highly correlated with the age parameter ($P < 0.001$). The high value of these features showed maximum entropy in the dynamic content of wall vibration signals.

In another section, information on RF echo phases was studied. The RF signal phase was extracted first and then the new phase-difference matrix of the RF signals throughout subsequent frames in a specific line was calculated. Finally, in order to investigate the complexity and irregularity, the entropy of the phase-difference was used. Results showed that average values of the entropy of phase-difference increase with age. To consider the direct relationship of phase-difference with artery wall motion velocity, it can be inferred that while age and wall stiffness increase, the motion of the wall is irregular and shows chaotic behavior.

The proposed method for measuring wall vibrations and phase information of RF echo can potentially be used for the diagnosis of atherosclerosis at initial stages, and also for evaluating the development of atherosclerosis in a shorter time than other methods. This method is also effective in preventing atherosclerosis. Using this method, the effects of risk factors in atherosclerosis such as diabetes, smoking, hyperlipidemia, and being inactive can be investigated.

4. Conclusion

The aim of this study was twofold. Primarily, we propose a noninvasive method to extract carotid artery wall vibrations, which can be more useful in evaluating elasticity of artery walls and the diagnosis of atherosclerosis in initial stages compared to existing methods. Second, we aimed to determine whether the changes of artery wall vibrations are related to the wall stiffness, for which the effect of age on wall vibration was used. To this end, the effects of age on nonlinear features of vibrations and entropy of the phase-difference of RF echo were used and it was concluded that these features were highly correlated with age; while age increased, the values of these features also increased.

Acknowledgment

The authors acknowledge Dr. Yusefi Rizi for her valuable help in data acquisition.

Ethics approval

Study approval was obtained from the Human Research Ethics Committee of the Islamic Azad University, Science and Research Branch, Department of Biomedical Engineering.

References

[1] Lee RT, Libby P. The unstable atheroma. Arterioscl Thromb Vas 1997; 17: 1859–1867.

[2] Kondo K, Nemoto M, Harada N, Fukushima D, Masuda H, Sugo N. Comparison between quantitative stiffness measurements and ultrasonographic findings of fresh carotid plaques. Ultrasound Med Biol 2017; 43: 138-144.

[3] Kiechl S, Willeit J. The natural course of atherosclerosis. Part I: Incidence and progression. Arterioscl Thromb Vas 1999; 19: 1484–1490.

[4] Ciccone MM, Scicchitano P, Zito A, Agati L, Gesualdo M, Mandolesi S, Carbonara R, Ciciarello F, Fedele F. Correlation between coronary artery disease severity, left ventricular mass index and carotid intima media thickness, assessed by radio-frequency. Cardiovasc Ultrasoun 2011; 9: 32.

[5] Smedby O. Do plaques grow upstream or downstream? An angiographic study in the femoral artery. Arterioscl Throm Vas 1997; 17: 912–918.

[6] Jaffer FA, O'Donnel CJ, Larson MG, Chan SK, Kissinger KV, Kupka MJ, Salton C, Botnar RM, Levy D, Manning WJ. Age and sex distribution of subclinical aortic atherosclerosis: a magnetic resonance imaging examination of the Framingham heart study. Arterioscl Throm Vas 2002; 22: 849–854.

[7] Wendelhag I, Wiklund O, Wikstrand J. On quantifying plaque size and intima-media thickness in carotid and femoral arteries: comments on results from a prospective ultrasound study in patients with familial hypercholesterolemia. Arterioscl Throm Vas 1996; 16: 843–850.

[8] Larsson M, Heyde B, Kremer F, Brodin LA, D'Hooge J. Ultrasound speckle tracking for radial, longitudinal and circumferential strain estimation of the carotid artery – An in vitro validation via sonomicrometry using clinical and high-frequency ultrasound. Ultrasonics 2015; 56: 399-408.

[9] Khan A, Sikdar S, Hatsukami T, Cebral J, Jones M, Huston J, Howard G, Lal BK. Noninvasive characterization of carotid plaque strain. Vascular Surg 2017; 65: 1653-63.

[10] Czernuszewicz JT, Homeister WJ, Caughey CM, Farber AM, Fulton JJ, Ford P, Marston AW, Vallabhaneni R, Nichols CT, Gallippi MC. Non-invasive in vivo characterization of human carotid plaques with acoustic radiation force impulse ultrasound: comparison with histology after endarterectomy. Ultrasound Med Biol 2015; 41: 685-697.

[11] Huang C, He Q, Huang M, Huang L, Zhao X, Yuan C, Luo J. Non-invasive identification of vulnerable atherosclerotic plaques using texture analysis in ultrasound carotid elastography: an in vivo feasibility study validated by magnetic resonance imaging. Ultrasound Med Biol 2017; 43: 817-830.

[12] Hallock P. Arterial elasticity in man in relation to age as evaluated by the pulse wave velocity method. Arch Intern Med 1934; 54: 770–798.

[13] Giannattasio C, Failla M, Emanuelli G, Grappiolo A, Boffi L, Corsi D, Mancia G. Local effects of atherosclerotic plaque on arterial distensibility. Hypertension 2001; 38: 1177-1180.

[14] Kanber B, Hartshorne TC, Horsfield MA, Naylor AR, Robinson TG, Ramnarine KV. Wall motion in the stenotic carotid artery: association with greyscale plaque characteristics, the degree of stenosis and cerebrovascular symptoms. Cardiovasc Ultrasoun 2013; 11: 37.

[15] Cecelja M, Chowienczyk P. Role of arterial stiffness in cardiovascular disease. JRSM Cardiovascular Disease. 2012; 1: 11.

[16] Hasegawa H, Kanai H, Hoshimiya N, Chubachi N, Koiwa Y. Accuracy evaluation in the measurement of a small change in the thickness of arterial walls and the measurement of elasticity of the human carotid artery. Jpn J Appl Phys 1998; 37: 3101-3105.

[17] Kanai H, Sato M, Koiwa Y, Chubachi N. Transcutaneous measurement and spectrum analysis of heart wall vibrations. IEEE T Ultrason Ferr 1996; 43: 791-810.

[18] Kanai H, Koiwa Y. Real-time velocimetry for evaluation of change in thickness of arterial wall. Ultrasonics 2000; 38: 381-386.

[19] Hasegawa H, Kanai H, Koiwa Y. Modified phased tracking method for measurement of change in thickness of arterial wall. Jpn J Appl Phys 2002; 41: 3563-3571.

[20] Kanai H, Haseqawa H, Ichiki M, Tezuka F, Koiwa Y. Elasticity imaging of atheroma with transcutaneous ultrasound: preliminary study. Circulation 2003; 107: 3018-3021.

[21] Smedby R. Do plaques grow upstream or downstream? An angiographic study in the femoral artery. Arterioscl Throm Vas 1997; 17: 912–918.

[22] Jaffer FA, O'Donnel CJ, Larson MG, Chan SK, Kissinger KV, Kupka MJ, Salton C, Botnar RM, Levy D, Manning WJ. Age and sex distribution of subclinical aortic atherosclerosis: a magnetic resonance imaging examination of the Framingham heart study. Arterioscl Throm Vas 2002; 22: 849–854.

[23] Wendelhag I, Wiklund O, Wikstrand J. On quantifying plaque size and intima-media thickness in carotid and femoral arteries: comments on results from a prospective ultrasound study in patients with familial hypercholesterolemia. Arterioscl Throm Vas 1996; 16: 843–850.

[24] Moradi M, Abolmaesumi P, Isotalo P, Siemens D, Sauerbrei E, Mousavi P. Detection of prostate cancer from RF ultrasound echo signals using fractal analysis. In: Proceedings of the 2006 IEEE EMBC. New York, NY, USA: IEEE, 2006. pp. 2400-2403.

[25] D'Hooge J. Interaction of ultrasonic waves and tissues: modeling, simulations and applications. PhD, Louven University, Louven, Belgium, 1999.

[26] Wagner RF, Insana MF, Brown DG. Statistical properties of radio-frequency and envelope-detected signals with applications to medical ultrasound. J Opt Soc Am A 1987; 4: 910-922.

[27] Dydenko I, Friboulet D, Gorce JM, D'Hooge J, Bijnens B, Magnin I. Towards ultrasound cardiac image segmentation based on the radiofrequancy signal. Journal of Medical Image Analysis 2003; 7: 353-367.

[28] Laurent S, Marais L, Boutouyrie P. The noninvasive assessment of vascular aging. Can J Cardiol 2016; 32: 669-679.

[29] Sunagawa K, Kanai H, Koiwa Y, Nitta K, Tanaka M. Simultaneous measurement of vibrations on the arterial wall downstream and upstream from an atherosclerotic lesions. In: Proceedings of the 1999 IEEE Ultrasonics Symposium; Tahoe, NV, USA. New York, NY, USA: IEEE, 1999. pp. 1507–1510.

[30] Zavar M, Rahati S, Akbarzadeh TM, Ghasemifard H. Evolutionary model selection in a wavelet-based support vector machine for automated seizure detection. Expert Syst Appl 2011; 38: 10751–10758.

[31] Garnett PW. Chaos Theory Tamed. 1st ed. Washington, DC, USA: Joseph Henry Press, 1997.